SPALLATION NEUTRON SPECTRUM
ON A MASSIVE LEAD/PARAFFIN TARGET
IRRADIATED WITH 1 GEV PROTONS

Адам И. и др.

E1-2004-16

Спектр нейтронов, образованных в массивной свинцовой мишени,
окруженной парафином и облучаемой протонами
с энергией 1 ГэВ

С помощью пороговых детекторов ^{209}Bi, ^{197}Au, ^{59}Co, ^{115}In, ^{232}Th получен спектр нейтронов, рождающихся в реакциях расщепления внутри цилиндрической свинцовой мишени ($L \times R = 20 \times 4$ см), окруженной толстым (6 см) слоем парафина и облучаемой пучком протонов с энергией 1 ГэВ, полученным на нуклотроне ЛВЭ ОИЯИ.

Измерены спектры гамма-лучей, испускаемых радиоактивными остаточными ядрами. Определены и сравниваются с монте-карловскими расчетами на основе каскадно-испарительной модели «Каскад» (с учетом деления) относительные вероятности реакций $(n, xn), (n, xnyp), (n, p), (n, \gamma)$.

Работа выполнена в Лаборатории ядерных проблем им. В. П. Джелепова ОИЯИ.

Adam J. et al.

E1-2004-16

Spallation Neutron Spectrum on a Massive Lead/Paraffin Target
Irradiated with 1 GeV Protons

The spectra of gamma-ray emitted by decaying residual nuclei, produced by spallation neutrons with $(n, xn), (n, xnyp), (n, p), (n, \gamma)$ reactions in activation threshold detectors — namely, ^{209}Bi, ^{197}Au, ^{59}Co, ^{115}In, ^{232}Th, were measured in the Laboratory of Nuclear Problems (LNP), JINR, Dubna, Russia. Spallation neutrons were generated by bombarding a 20 cm long cylindrical lead target, 8 cm in diameter, surrounded by a 6 cm thick layer of paraffin moderator, with a 1 GeV proton beam from the Nuclotron accelerator. Reaction rates and spallation neutron spectrum were measured and compared with CASCADE code calculations.

The investigation has been performed at the Dzhelepov Laboratory of Nuclear Problems, JINR.

INTRODUCTION

For the last decade Accelerator Driven sub-critical Systems (ADS) ([1, 2] and references therein), where an accelerator is coupled with a reactor, have been considered as a promising and challenging task for transmutation of long-lived radioactive waste and for energy production. This system is significantly safer, due to its sub-criticality, than conventional critical reactors. Spallation neutrons are generated by bombardment of heavy targets such as Pb, Pb-Bi(eutectic), Hg, etc. with protons, and react with fuel material (Th, U, etc.) or with exposed radioactive waste from conventional reactors or weapons. For the design of ADS it is important to study neutron spectra and details of nuclear reactions induced by neutrons. Many experimental results are available for thin targets (e. g. [3]) but for massive targets additional studies of neutron spectra and cross-section are needed to design real ADS and to improve transport codes.

When using thorium as a nuclear ADS fuel the study of the production of problematic transthorium nuclides is essential. There are a few experimental neutron production cross-sections available for thorium, however, some results are in contradiction [4, 5]. Therefore, in a side-experiment we also irradiated some Th-metal with primary spallation neutrons.

Some recent experimental results [3] for thin targets, obtained by the group of Yu. V. Trebukhovsky on double differential neutron production cross-sections for different targets, and their comparison with the CASCADE, CEM97, and LAHET simulation codes show that calculated neutron multiplicity values are somewhat higher than experimental values, in particular at small angles. From this point of view it may be important to study spallation neutron spectra (spatial and energy distribution) as well as total neutron yields in order to improve the physics implemented in simulation codes.

1. EXPERIMENTAL SETUP AND METHOD OF MEASUREMENT

The sketched setup of the GAMMA-2 experiment is given in Fig. 1. A target consisting of 20 lead discs, each 1 cm in thickness and 8 cm in diameter and surrounded by a 6 cm paraffin moderator was irradiated with a 1 GeV proton
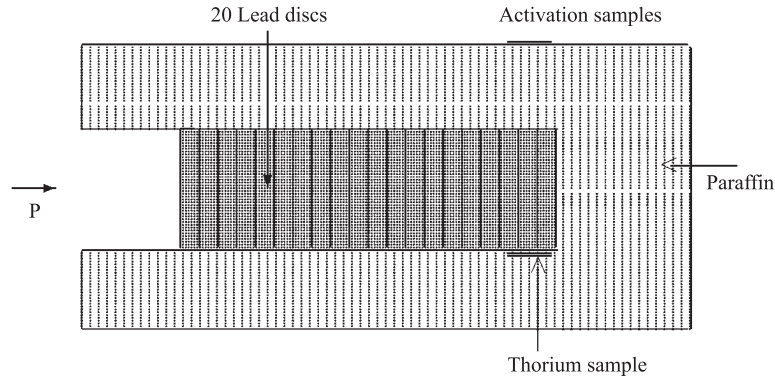
1

Fig. 1. The experimental setup with a lead target and a paraffin moderator

beam extracted from the Nuclotron in the Laboratory of High Energies (LHE) at JINR for 5 hours and 29 minutes. Activation samples of ^{209}Bi, ^{197}Au, ^{59}Co, ^{115}In were placed on the top of the paraffin surface as shown in Fig. 1. ^{232}Th sample wrapped in thin aluminium was placed directly on the surface of the lead target inside the paraffin. The ^{232}Th sample was prepared by Bhaba Atomic Research Center (Mumbai, India) and the other samples were supplied by the University of Rajasthan and LNP.

The physical characteristics of these samples are given in Table 1.

Table 1: **Characteristics of the irradiated samples**

Target	Mass, g	Thickness, g/cm^2	Thickness, mm
^{209}Bi	3.1	2.44	2.50
^{179}Au	1.19	1.06	0.55
^{115}In	0.11	0.07	0.09
^{59}Co	3.33	3.56	4.0
^{232}Th	0.013	0.0018	0.0046

The proton beam was monitored by thin Al foils situated approximately 60 cm before the target to avoid the influence of backwards emitted neutrons produced from the target. The intensity of protons was obtained with ^{27}Al(p, $3pn$)^{24}Na reaction using a cross-section of 10.51(17) mb [6] (the uncertainty in brackets refers to the last digit). The influence of the ^{27}Al(n, α)^{24}Na reaction was not taken into account as it is negligible under the experimental conditions [7]. The variation of the beam intensity during irradiation is presented in Fig. 2. It is

2

clear from Fig. 2 that the assumption of a constant intensity is not justified when calculating the decay of products during irradiation. We have taken into account the correction for the fluctuation and interruption of the beam. This correction was done for all the product nuclei, which is particularly important for product nuclei having a half-life shorter than the irradiation time (for example, the correction to ^{201}Bi ($T_{1/2} = 108$ min) was 25%). The proton flux on the lead target was estimated as $10.90(65)10^8$ protons/s, as determined by the monitoring reaction ^{27}Al(p, $3pn$)^{24}Na taking into account the beam fluctuations and coincidence summing.
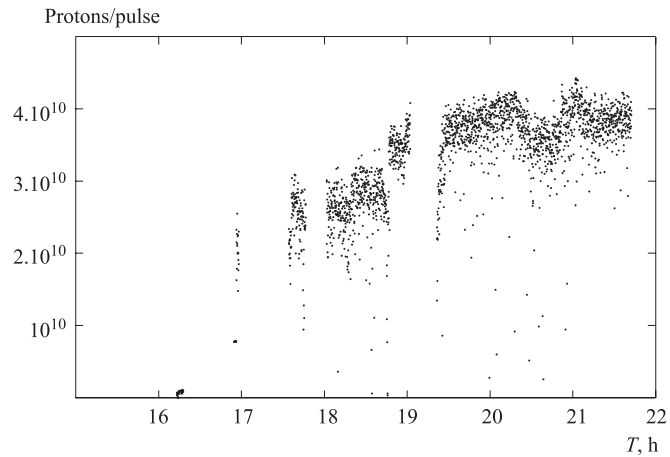

Fig. 2. Variation of the beam intensity during irradiation. Each dot shows one pulse of particular intensity.

Measurement of spectra of gamma-rays emitted by the above mentioned samples was started at LNP three hours after the irradiation and 11–12 spectra from each sample were measured with time intervals up to 15 days after the irradiation. The measurement of spectra from the thorium sample was started 19 hours after the irradiation and measured up to one month with appropriate time intervals. Samples irradiated with spallation neutrons were measured by using a High Purity Germanium (HPGe) detector with 28% relative efficiency and an energy resolution of 2 keV (FWHM ^{60}Co at 1332 keV) at LNP. Due to the low activity in the samples, measurements were taken at a 0 cm distance from the detector endcap. Recording of gamma-ray spectra was carried out with a high rate multichannel buffer SPECTRUM MASTER 921.

The DEIMOS Program [8] was used in an interactive mode for spectrum analysis. This program determined the areas and positions of peaks taking into account the background level. Exact energies of the peaks were found using

suitable calibration points. The program also gave a tentative list of product isotopes using a rich library (containing energy, intensity per decay, and half-life of the isotopes).

After spectrum handling the data were cleaned from the internal and external background lines. The corrected intensities of the gamma-lines were used to determine the half-lives of the product nuclei, including complex lines. Identification of the products was based on the energies and intensities of the gamma-lines as well as on half-lives as given in Atomic Data and Nuclear Data Tables [9,10]. The reaction rates R [proton^{-1} atom^{-1}] of product nuclei were calculated taking into account the corrections for peak efficiency of the HPGe detector, for coincidence summing effect, for self-absorption, and for decay during irradiation (in consideration of the fluctuation of beam current during the irradiation).

The reaction rate R [proton^{-1} atom^{-1}] is related to the neutron flux as follows [11]:

$$R = \int_{E_{\text{th}}}^{\infty} \sigma(E)\phi(E)dE. \tag{1}$$

Here, $\phi(E)$ is a neutron flux (neutron/(cm$^2 \cdot$MeV$\cdot p$)) passing through the samples, E_{th} is the threshold neutron energy for the observed reaction in the particular sample.
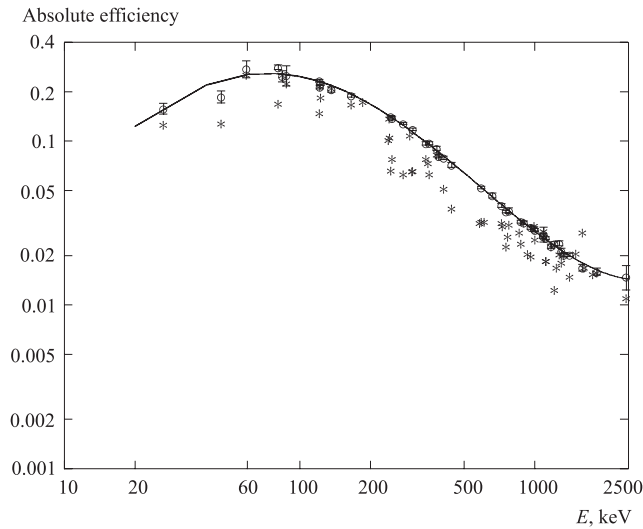

Fig. 3. Absolute efficiency at a 0 cm distance and the least squares fit. Asterisks (*) are raw data and circles (o) after coincidence summing correction

4

As mentioned above, we have measured the activation samples at a 0 cm distance from the detector, so we have measured the efficiency of the detector at 0 cm and 25 cm distances from the detector using calibrated sources of ^{137}Cs, ^{109}Cd, ^{139}Ce, ^{88}Y, ^{113}Sn, ^{152}Eu, ^{154}Eu, ^{228}Th, ^{241}Am, ^{54}Mn, ^{60}Co and applied the corresponding coincidence summing corrections, neglecting coincidence summing at 25 cm. The curve for absolute efficiency at a 0 cm sample distance with and without coincidence summing corrections is shown in Fig. 3. We have taken into account the corrections for all observed product nuclei following [12]. Corrections were up to 40% (e. g. ^{204}Bi) for such a close geometry.

2. MODELLING AND DISCUSSION

The experimental reaction rates are compared with values calculated by the CASCADE [13] code in Table 2, where E_{th} is the threshold energy, E_γ is the observed gamma-ray energy, I_γ is the emission rate (intensity) of this gamma-ray per decay, $T_{1/2}$ is the half-life of produced nuclei, R_i^{calc} is the calculated reaction rate for ith reaction by CASCADE code and R_i^{exp} is the experimental reaction rate.

Table 2: **Measured and calculated reaction rates**

Target/Product	E_{th}, MeV	$T_{1/2}$	E_γ, keV	I_γ, %	R_i^{cal}, 10^{-29}	R_i^{exp}, 10^{-29}	Uncertainty, $\pm$%
^{209}Bi $(n, 4n)^{206}$Bi	22.55	6.243 d	803.1 881.01	98.9 66.16	5.28	1.47 1.54 1.49[1]	5.8 16.1 5.8
^{209}Bi$(n, 5n)^{205}$Bi	29.62	15.31 d	703.4 1764.3	31.0 32.47	3.00	1.34 1.40 1.35[1]	6.8 8.6 6.6
^{209}Bi$(n, 6n)^{204}$Bi	38.13	11.30 h	899.2 983.98	99.2 58.76	1.48	0.98 0.90 0.93[1]	8.1 7.7 7.1
^{209}Bi$(n, 7n)^{203}$Bi	45.37	11.76 h	820.5 825.2	29.7 14.6	1.15	0.83 0.85 0.83[1]	7.8 9.9 7.4
^{209}Bi$(n, 9n)^{201}$Bi	61.69	1.8 h	629.1	24.0	0.48	0.49	18.6
^{232}Th $(n, \gamma)^{233}$Th[2]		26.967 d	300.12 311.98	06.6 38.6		917.0 997.0 980.0[1]	8.5 6.2 6.1
^{197}Au$(n, 2n)^{196}$Au	8.113	6.183 d	355.73 333.03	87 22.9	8.58	3.54 3.57 3.55[1]	6.15 7.0 6.0

Table 2 (continued)

Target/Product	E_{th}, MeV	$T_{1/2}$	E_γ, keV	I_γ, %	R_i^{cal}, 10^{-29}	R_i^{exp}, 10^{-29}	Uncertainty, $\pm\%$
^{197}Au$(n, 4n)^{194}$Au	23.205	38.02 h	328.4	60	4.77	1.66	7.0
^{197}Au$(n, 6n)^{192}$Au	38.939	4.94 h	296.0 316.5	22.3 58.0	2.35	1.29 1.12 1.15[1]	16.9 10.1 9.7
^{197}Au$(n, 7n)^{191}$Au	45.97	3.18 h	586.5	17	1.21	0.60	7.9
^{197}Au$(n, \gamma)^{198}$Au		2.695 d	411.80 675.88	95.5 0.8		438.0 446.0 439.0[1]	5.3 6.7 5.3
^{115}In$(n, 5n)^{111}$In	33.74	2.8047 d	171.4 245.35	90.24 94.0	2.06	0.90 0.91 0.90[1]	8.5 8.4 7.4
^{115}In$(n, 6n)^{110}$In	43.82	4.9 h	657.75	98.29	0.48	0.33	16.2
^{115}In$(n, 7n)^{109}$In	51.96	4.2 h	203.5	73.5	0.32	0.31	12.6
^{59}Co$(n, 2n)^{58}$Co	10.64	70.82 d	810.75	99.45	6.45	1.96	5.9
^{59}Co$(n, 3n)^{57}$Co	19.37	271.79 d	122.06 136.47	85.5 10.68	3.15	0.31 0.33 0.32[1]	6.8 13.0 6.7
^{59}Co$(n, 4n)^{56}$Co	30.96	77.27 d	846.75 1238.3	99.9 66.95	0.11	0.11 0.11 0.11[1]	8.8 16.5 8.6
^{59}Co$(n, 5n)^{55}$Co	41.24	17.53 h	931.5	75	.019	0.009	11.6
^{59}Co$(n,\gamma)^{60}$Co		1925.1 d	1173.2 1332.5	99.97 99.98		79.9 80.1 80.0[1]	5.8 5.8 5.8
^{59}Co $(n, p)^{59}$Fe	0.796	44.503 d	1099.22 1291.56	56.5 43.2		0.17 0.19 0.17[1]	8.1 8.5 7.3
^{59}Co$(n, 2p6n)^{52}$Mn		5.591 d	1434.09 935.54	100.0 94.9		0.45 0.48 0.46[1]	7.4 8.5 7.3

[1] Weighted average value.
[2] We observed ^{233}Pa as decay daughter of primary product ^{233}Th.

Uncertainties in the table are calculated from the statistical error of the spectral data plus the 6% uncertainty of the beam intensity measured via the ^{27}Al(p, $3pn$)^{24}Na monitor reaction. Weighted average reaction rates are presented in case that two or three lines were observed from the same nuclide. For calculating the average only statistical uncertainties have been taken into account.

Model calculations were performed by Monte Carlo simulation, using the CASCADE code, to obtain the theoretical spallation neutron spectra and reaction rates (other calculations were published [14] using the same code for the above mentioned setup, where one can find more details about the spatial and energy spectra of the neutrons). The CASCADE code considers three stages of reactions for calculation:

— Intranuclear cascade stage, originally developed at Dubna: in this part of the calculation, primary particles can be rescattered and they may produce secondary particles several times prior to absorption or escape from the target.

— Pre-equilibrium stage: in this part of the reaction, relaxation of the nuclear excitation is treated according to exciton model of pre-equilibrium decay. Proton, neutron, deuterium, tritium, ^{3}He and ^{4}He are considered as emitted particle in the pre-equilibrium and in the subsequent equilibrium stage.

— Equilibrium stage: this part considers particle evaporation/fission of the thermally equilibrated nucleus. The code uses 26-group constants [15] for cross-sections below 10.5 MeV and for higher energies, cross-sections are taken from [16, 17]. The code traces the protons down to 10 MeV and π^+ mesons down to 2 MeV. At lower energies these particles are considered as stopped. Low-energy π^- mesons are captured in a nucleus creating new intranuclear cascades. Neutrons are traced down to thermalization.

We simulated 10^5 cascades (with the uncertainty in the calculation less than 1%) to calculate spectra and cross-section for different channels of the reactions. We calculated the probabilities for different reactions (n, xn) and then normalized to the total inelastic cross-section taken from [16, 17] and obtained the cross-section. An example of cross-section for ^{209}Bi(n, $4n$) ^{206}Bi reaction calculated with the CASCADE code and the comparison with experimental cross-sections [11] is given in Fig. 4 below. The similar procedure was adopted to calculate the cross-section by the CASCADE code for all the samples.

For the calculation of theoretical reaction rate we used $dE \approx \Delta E = 2$ MeV for the integration in Eq. (1).

One can see from Table 2 that for bismuth isotopes produced below a threshold energy of 50 MeV the calculated reaction rates are 2–3 times higher than the experimental reaction rates, but numbers agree within experimental uncertainties at higher neutron energies. Such a trend was observed for all the samples. A similar disagreement with other experimental data [3] was also observed in our previous calculations, thus pointing at a systematic trend.
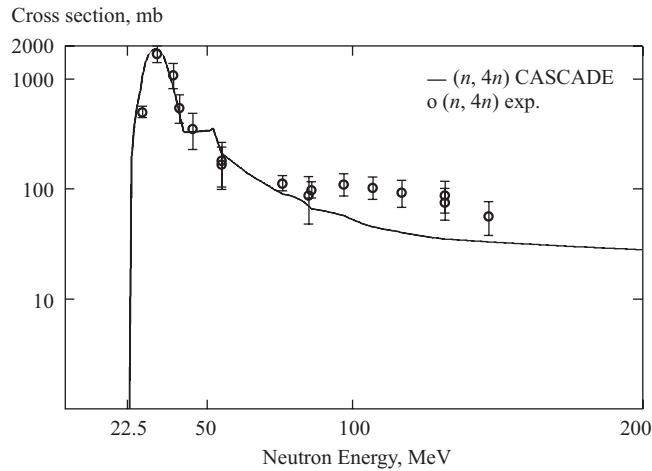
7

Fig. 4. The similar procedure was adopted to calculate the cross-section by the CASCADE code for all the samples

In the spectra taken from the ^{232}Th sample we clearly observed ^{233}Pa which is the first daughter of the single neutron capture product; this finding qualitatively indicates that even directly on the surface of the primary lead target one can find low-energy neutrons in abundance.

In case of ^{59}Co, ^{59}Co(n, $2p6n$)^{52}Mn reaction gives evidence of spallation reaction, i.e, the evidence of high-energy neutrons even after moderation by paraffin.

3. UNFOLDING OF NEUTRON SPECTRA

Experimental neutron spectra were deduced using the following procedures: on the right-hand side of Eq. (1) there are two energy-dependent variables — the cross-section and the neutron fluence. In the first analysis we assume a constant neutron fluence over some energy and integrate for the cross-section (Analysis 1 below) and for the second analysis we follow Ref. [18] and consider the cross-section as constant and integrate for the neutron fluence (Analysis 2 below).

Analysis 1. A constant neutron fluence is assumed from the threshold energy for the (n, xn) reaction with the nighest value of x to the maximum possible energy of neutrons, which is theoretically almost up to the incident proton energy. The maximum neutron energy calculated by the CASCADE code is only around 600 MeV, however, this difference in the maximum neutron energy effects the

8

calculated spectrum only negligibly because the cross-section for higher neutron energies is very small (see Fig. 4, the cross-section of Bi). The fluence from the threshold of the $(n, (x{-}1)n)$ reaction to the threshold of the (n, xn) reaction is again assumed to be constant and one can calculate the respective part of the spectrum, and so on. In this way one successively reaches the lower energy end of the spectrum. For example, one obtains the fluence $\phi(9)$ from Eq. (2) and then puts this value into Eq. (3) to calculate fluence $\phi(8)$ etc. (see below the method of calculation in Eqs. (2)–(4)).

$$R_9^{\text{exp}} = \phi(9) \int_{E_{\text{th}}(n,9n)}^{E_{\text{max}}} \sigma_9(E)dE, \tag{2}$$

$$R_8^{\text{exp}} = \phi(8) \int_{E_{\text{th}}(n,8n)}^{E_{\text{th}}(n,9n)} \sigma_8(E)dE + \phi(9) \int_{E_{\text{th}}(n,9n)}^{E_{\text{max}}} \sigma_8(E)dE, \tag{3}$$

$$R_7^{\text{exp}} = \phi(7) \int_{E_{\text{th}}(n,7n)}^{E_{\text{th}}(n,8n)} \sigma_7(E)dE + \phi(8) \int_{E_{\text{th}}(n,8n)}^{E_{\text{th}}(n,9n)} \sigma_7(E)dE+$$
$$+ \phi(9) \int_{E_{\text{th}}(n,9n)}^{E_{\text{max}}} \sigma_7(E)dE. \tag{4}$$

The spectrum above 22.5 MeV has been deduced using experimental cross-section and reaction rates for Bi sample, from 8.4 to 22.5 MeV the spectrum is obtained using $^{197}\text{Au}(n,2n)^{196}\text{Au}$ reaction. We used $^{59}\text{Co}(n,p)^{59}\text{Fe}$ reaction from 3.5 (though the theoretical neutron energy threshold for this reaction is 0.8 MeV but the experimental threshold is 3.5 MeV) to 8.4 MeV region. Experimental cross-sections for all the reactions are taken from [11, 19].

Analysis 2. The second approach to obtain the spectra is described in Ref. [18], where the procedure shall be presented here only for completeness.

$$R_i^{\text{exp}} = \sigma_i^{\text{eff}} \int_{E_i^{\text{eff}}}^{\infty} \phi(E)dE, \tag{5}$$

where

$$E_i^{\text{eff}} = E_i^{\text{th}}. \tag{6}$$

The neutron fluence $\phi(E)$ used in Eq. (5) is the theoretical fluence, all the notations are the same as above. Thus, in this approach one must start with the theoretical neutron spectrum and calculate σ_i^{eff}, which is the effective cross-section for the particular reaction. Thus, one gets the function $F(E_i^{\text{eff}})$ $[n/(\text{cm}^2\cdot p)]$ as an integral of the neutron spectrum

$$F(E_i^{\text{eff}}) = \frac{R_i^{\text{exp}}}{\sigma_i^{\text{eff}}} \tag{7}$$

and one can get the general formulae

$$F(E) = \int_E^\infty \phi(E')dE', \tag{8}$$

$$\phi(E) = -\frac{dF(E)}{dE}. \tag{9}$$

In this analysis, one starts with the theoretical neutron fluence to calculate the effective cross-section and later to calculate the integral function $F(E)$ of the neutron fluence. The function $F(E)$ is shown in Fig. 5.
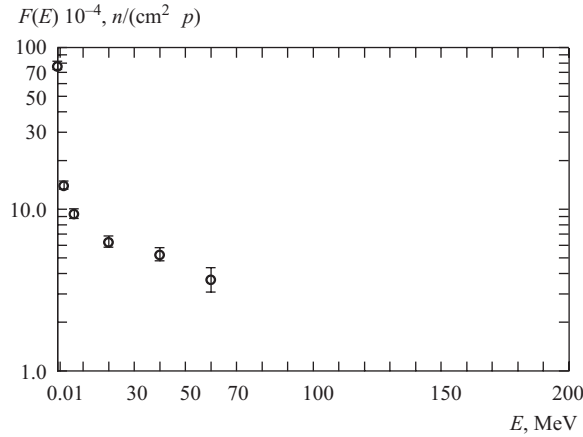
Fig. 5. The integral function $F(E)$ of neutron spectra

One can then obtain the «experimental» spectrum by differentiating the integral function $F(E)$. In this way the spectrum will not be really experimental but it is strongly influenced by the initial theoretical fluence or, in other words, the differentiation of the integral function will always be in agreement with the theoretical one (see Fig. 6). In our opinion, this method is not viable for the generation of the experimental neutron spectrum and for comparison with theory. We prefer Analysis 1 in which the product cross-section is well known with certain experimental uncertainties and the neutron spectrum is completely deduced from these experimental values. A comparison of calculated and deduced neutron fluences obtained by both analyses is given in Fig. 6.
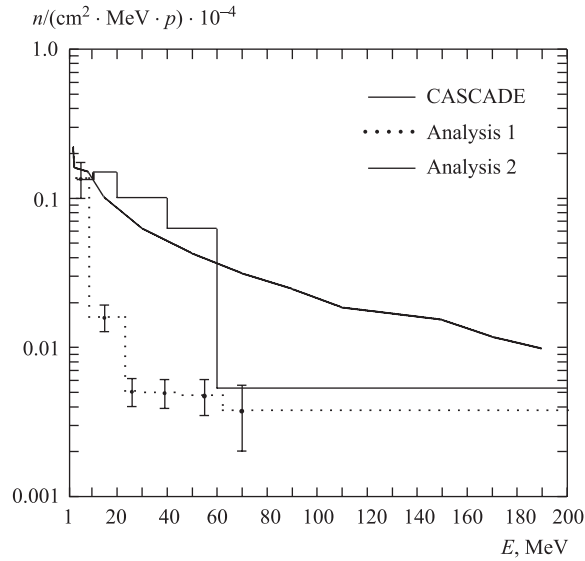
$n/(\text{cm}^2 \cdot \text{MeV} \cdot p) \cdot 10^{-4}$

Fig. 6. Comparison of experimentally deduced and calculated neutron spectra

CONCLUSIONS

From Table 2 it is clear that the calculated reaction rates are 2–3 times higher than the experimental ones for products where the reaction threshold energy E_{th} is in the range 10–50 MeV and it is in agreement in the higher energy region. We calculated the production cross-section by the CASCADE code for (*n, xn*) reactions and compared with experimental data [11]. From Fig. 6 one can see that the experimental neutron yield is significantly smaller than the neutron yield calculated by the CASCADE code. This finding is in agreement with our previous results [3], where such a disagreement was also observed for neutrons created in proton–Pb collisions at $E = 1$ and 1.6 GeV in thin targets. The CASCADE code may need improvement but we are now unable to say the exact reason of this disagreement.

REFERENCES

1. *Bowman C. D. et al.* // Nucl. Instr. Meth. A. 1992. V. 320. P. 336.
2. *Carminata F. et al.* // CERN report CERN/AT/93-47(ET). 1993.

3. *Trebukhovsky Yu. V. et al.* // ITEP-3. 2003; Yad. Fiz. (accepted)

4. *Kuzminov B. D., Manokhin V. N.* // Nucl. Const. 1997. V. 3–4. P. 41.

5. *Manokhin V. N., Odano N., Hasegawa A.* JAERI–DAta /Code 2001-019.

6. *Cumming J. B.* // Ann. Rev. Nucl. Sci. 1963. V. 13. P. 261;
   Westmeier W. et al. // Radioachimica Acta (submitted) (private communication).

7. *Wan J. -S. et al.* // Nucl. Instr. Meth. B. 1999. V. 155. P. 110.

8. *Frana J., Radioanal J.* // Nucl. Chem. 2003. V. 3(257). P. 583.

9. *Reus U., Westmeier W.* // At. Data Nucl. Data Tables. 1983. V. 29.

10. http://nucleardata.nuclear.lu.se/nucleardata/toi/radSearch.asp

11. *Kim E. et al.* // Nucl. Sci. Eng. 1998. V. 129. P. 209.

12. *Debertin K., Schotzig U.* // Nucl. Instr. Meth. 1979. V. 158. P. 471.

13. *Barashenkov V. S.* // Comp. Phys. Commun. 2000. V. 126. P. 28.

14. *Barashenkov V. S. et al.* JINR Preprint E9-2003-55. Dubna, 2003; Nucl. Instr. Meth. B (in press).

15. *Abagan L. P. et al.* Group constants for reactor and shielding calculations. M.: Energoatomizdat, 1981 (in Russian).

16. *Barashenkov V. S.* Cross-sections of interactions of particles and nuclei with nuclei. Dubna, 1993 (in Russian).

17. *Barashenkov V. S., Gudowski W., Polanski A.* JINR, E2-99-206. Dubna, 1999.

18. *Martsynkevich B. A. et al.* JINR, P1-2002-65. Dubna, 2002 (in Russian).

19. http://www-nds.iaea.org/exfor/

Редактор *Н. С. Скокова*